processes

MDPI

Article

Aggregation of Air Conditioning Loads in Building Microgrids: A Day-Ahead and Real-Time Control Strategy Considering User Privacy Requirements

Jinjin Ding [1], Wangchao Dong [1], Bin Xu [1], Dan Hu [1], Zheng Tian [2,*], Donglin Qin [2] and Hongbin Wu [2]

[1] State Grid Anhui Electric Power Research Institute, Hefei 230601, China; djinjin123@126.com (J.D.); dwchhf@live.com (W.D.); xubin1980@sina.com (B.X.); hd8158@sina.com (D.H.)
[2] School of Electrical Engineering and Automation, Hefei University of Technology, Hefei 230009, China; hfutqingdonglin@163.com (D.Q.); hfwuhongbin@hfut.edu.cn (H.W.)
* Correspondence: tz18326213220@163.com

Abstract

Air conditioning loads play a critical role in maintaining the supply–demand balance of building microgrids (BMGs), yet their distributed nature and volatile response may undermine secure and stable operation. This paper proposes a day-ahead and real-time aggregated control strategy for BMG air conditioning loads with user privacy protection. First, an approximate aggregation model is developed based on building heat transfer characteristics, and the aggregated response potential is evaluated by jointly considering user comfort and willingness. Second, without sharing fine-grained user information, a Building Microgrid Operator (BMO)–Load Aggregator (LA) day-ahead distributed-scheduling model is formulated and solved using the alternating direction method of multipliers (ADMM). Finally, to address load fluctuations caused by heterogeneous initial indoor temperature distributions, a real-time control strategy based on State-Queueing (SQ) temperature-state pre-transfer is proposed. Case studies show that, compared with the baseline scheme, the proposed method reduces the system operating cost from CNY 50,694.58 to CNY 47,131.64, a 7% decrease, and decreases load shedding from 1466.35 kWh to 257.31 kWh, an 82% decrease. Meanwhile, the real-time control effectively suppresses power fluctuations in the early control stage, thereby improving both economic performance and response smoothness.

Keywords: air conditioning load; aggregated control; privacy protection; building microgrid; day-ahead scheduling; real-time control

Check for updates

Academic Editor: Jiaqiang E

Received: 24 November 2025
Revised: 4 January 2026
Accepted: 11 January 2026
Published: 13 January 2026

Copyright: © 2026 by the authors. Licensee MDPI, Basel, Switzerland. This article is an open access article distributed under the terms and conditions of the Creative Commons Attribution (CC BY) license.

1. Introduction

Driven by the global energy transition and sustainable development goals, optimizing energy consumption in buildings has become a crucial approach to achieving energy conservation and emission reduction [1–3]. As one of the primary energy-consuming devices in buildings, air conditioning loads enable buildings to exhibit a certain level of demand-response capability while maintaining user comfort [4–7]. Therefore, optimizing electricity consumption strategies in buildings is key to unlocking the potential of air conditioning load control, and microgrid energy management provides a feasible solution to this challenge [8,9].

With the comprehensive deployment of distributed generation (DG), energy storage systems, and intelligent modules in buildings, the concept of the BMG has emerged.

The BMG system is managed by the BMO, which oversees unified energy consumption management, engages in electricity purchasing and selling transactions with the upper-level power grid, and adjusts its operational strategies to maximize economic benefits [10,11]. Air conditioning loads are primarily aggregated and regulated by the LA, contributing to the supply–demand balance within the system [12]. However, the BMO and LA are typically separate entities, and due to user privacy protection concerns, the LA does not share detailed user equipment information with the BMO [13,14]. Therefore, how to fully consider user privacy requirements while formulating rational energy consumption plans and implementing precise control of air conditioning loads is of great significance for enhancing energy efficiency, reducing consumption, and ensuring the secure and stable operation of BMG systems [15,16]. To this end, Ref. [17] proposes a decentralized energy management framework for privacy-preserving demand response in smart buildings, enabling individual users to participate in system-level optimization while retaining full control over their local operational data.

Currently, research on air conditioning load control in BMG systems can be broadly categorized into two main aspects: optimization scheduling and control strategies, based on the differences in application scenarios and regulation objectives.

In the research on air conditioning load optimization scheduling methods for BMG systems, the BMO needs to explore the response characteristics of air conditioning loads in depth to maximize their potential in system regulation, peak-shaving and valley-filling, and supply–demand balance, thereby formulating reasonable and effective scheduling plans [18,19]. Ref. [20] develops a centralized optimization scheduling model for BMGs, which comprehensively considers the management of heating, ventilation, and air conditioning (HVAC) units, lighting equipment, photovoltaic (PV) generation, and energy storage systems in each building. Ref. [21] proposes a real-time scheduling method for multiple BMGs based on model predictive control, effectively optimizing the energy consumption plans of HVAC systems in individual apartments and improving the matching performance between regional generation and consumption. To further enhance real-time scheduling efficiency, Ref. [22] applies Lyapunov optimization technology (LOT) to BMG scheduling, optimizing the total cost, thermal comfort cost, and charging/discharging strategies of batteries and electric vehicles through real-time dispatch, which has practical engineering significance. Ref. [23] investigates a residential multi-energy community with controllable heating, ventilation, and air conditioning (HVAC) systems and energy storage, and proposes a two-stage coordinated scheduling framework consisting of day-ahead planning and real-time correction. In both stages, a decentralized model predictive control scheme based on the alternating direction method of multipliers (ADMM) is employed to enable distributed scheduling of user-side HVAC and to mitigate uncertainty. Ref. [24] addresses the issue of source–load mismatch in high-penetration renewable energy systems by establishing a two-stage energy-trading framework for HVAC systems, incorporating day-ahead scheduling and intra-day real-time clearing to mitigate real-time power shortages in residential microgrids. At the air conditioning load scheduling level, existing optimization scheduling methods primarily rely on centralized algorithms. However, since the BMO and LA are typically separate entities, the issue of privacy protection in information exchange between them remains largely unexplored by scholars both domestically and internationally.

Air conditioning load control strategies focus more on the fine-grained regulation of aggregated or individual air conditioning units under different scenarios. These strategies primarily adopt Direct Load Control (DLC) methods, where control models are constructed by setting appropriate objective functions, decision variables, and constraints [25]. Ref. [26] thoroughly considers the power rebound effect of air conditioning loads before and after

demand response, establishing a reserve capacity–time evaluation framework and proposing a sequential control strategy that effectively improves the utilization efficiency of air conditioning loads as reserve resources. Ref. [27] introduces a novel alternating-current DLC mechanism that constrains regional generation capacity and directly controls users' air conditioning duty cycles, achieving peak load reduction while maintaining user comfort, with significant economic and environmental benefits. To enhance the flexibility of air conditioning control, Ref. [28] develops an SQ model based on air conditioning switching cycle characteristics, setting start–stop transition temperatures to regulate operational state changes, thereby realizing distributed rolling control of air conditioners. Ref. [29] proposes an Adaptive ON/OFF State-Switching (AOSS) control method for inverter-based air conditioning clusters, integrating the traditional SQ model into an Inverter Air Conditioning Load (IACL) cluster for short-term power control, demonstrating promising control performance. At the air conditioning load control level, while existing research strategies accommodate diverse control requirements across different scenarios, their control objectives are typically predetermined, resulting in a disconnection from the day-ahead scheduling layer. Moreover, they fail to adequately consider power fluctuations caused by the initial temperature distribution of air conditioning loads.

The above studies have achieved promising control performance in different scenarios, but have not realized the coordinated optimization of the scheduling and control layers. Therefore, to fully consider user privacy protection needs while balancing the differing interests of the BMO and users, this paper proposes a day-ahead and real-time air conditioning load aggregation and control strategy for BMG systems, incorporating user privacy requirements. At the day-ahead scheduling layer, a distributed-scheduling model based on ADMM is developed to address user privacy concerns, enabling energy consumption optimization under unknown global information. At the real-time control layer, a control strategy based on the SQ model temperature state pre-transition is proposed to mitigate response fluctuations caused by uneven initial temperature distributions among users, achieving coordination between the scheduling and control layers. The significant contributions of this study are summarized as follows:

(1) Day-ahead and real-time air conditioning load aggregation and control framework: To address the insufficient coordination between the air conditioning load scheduling and control layers, a collaborative framework for day-ahead and real-time air conditioning load aggregation and control is constructed. At the day-ahead scheduling layer, user privacy protection is fully considered, and a distributed-scheduling plan is formulated based on boundary information exchange between the BMO and LA. At the real-time control layer, the LA aims to minimize control time and designs a real-time air conditioning load control strategy that tracks the scheduling plan. The proposed framework effectively accounts for the diverse interests of multiple stakeholders while ensuring user privacy protection, enabling coordinated optimization of the scheduling and control layers.

(2) BMO-LA distributed scheduling: To address the BMO's computational burden and user privacy concerns, a day-ahead distributed optimization scheduling model is developed that considers the interests of both the BMO and LA. The model minimizes system operating costs and employs the ADMM algorithm, which ensures strong privacy protection and efficient parallel-computing capabilities, to iteratively solve the corresponding subproblems. The proposed model effectively reduces system operating costs and enables distributed optimization with unknown user global information.

(3) SQ-based pre-emptive control strategy: To mitigate power fluctuations caused by uneven initial air conditioning temperature distributions, a real-time air conditioning load control strategy based on the SQ-based pre-emptive control is proposed. By

adjusting the temperature modules in the SQ model based on their density distribution, this strategy aims to minimize control time while facilitating rapid transitions between temperature states, ensuring a balanced distribution of load levels across different modules. The proposed strategy effectively reduces power fluctuations in load clusters, achieving precise air conditioning load control.

The remainder of this paper is organized as follows. Section 2 introduces the overall framework for day-ahead and real-time air-conditioning load aggregation and control in BMG systems, and presents the approximate aggregation model considering building thermal characteristics and response-potential assessment, the day-ahead distributed scheduling model for BMO-LA with response potential, as well as the SQ-based pre-emptive control strategy for air-conditioning loads. Section 3 presents the case study and numerical results used to validate the proposed model. Finally, conclusions are summarized in Section 4.

2. Materials and Methods

2.1. Day-Ahead and Real-Time Aggregation and Control Framework for Air Conditioning Loads in Integrated BMG System

In multi-building integrated BMG systems, unified energy management is overseen by the BMO, which functions as both a production hub and a dispatch center, engaging in electricity-purchasing and -selling transactions with the upper-level power grid. While ensuring the stable operation of the system, the BMO further enhances economic benefits by optimizing its operational strategies. Direct participation of distributed building users in scheduling would increase system complexity. Therefore, the LA plays a crucial role in managing flexible loads such as air conditioning. By aggregating users' energy consumption data and executing the scheduling plans issued by the BMO, the LA centrally regulates the loads within its jurisdiction. This approach not only alleviates the scheduling burden on BMO but also facilitates efficient demand-response management.

In this paper, we focus on the coordinated optimization of supply and demand in integrated BMG systems and construct a day-ahead and real-time aggregation and control framework for air conditioning loads, as illustrated in Figure 1.

The day-ahead scheduling layer models the scheduling process by considering user privacy protection requirements and utilizes the aggregated response potential assessment from LA as boundary information. Based on the exchanged information between the BMO and LA, a distributed day-ahead scheduling plan is formulated to optimize energy consumption under unknown global information.

The real-time control layer focuses on the precise execution of scheduling decisions. In this layer, the LA acts as the executor within the proposed framework. It classifies air conditioning loads into multiple contract groups based on the adjustable temperature range and initial temperature distribution of users. To track the scheduling plan issued by the BMO, pre-emptive control based on the SQ model is applied, utilizing the density distribution of temperature modules. The primary objective of this control strategy is to minimize regulation time, ensuring coordinated, flexible, and precise real-time control of air conditioning loads while effectively tracking the scheduling decisions.

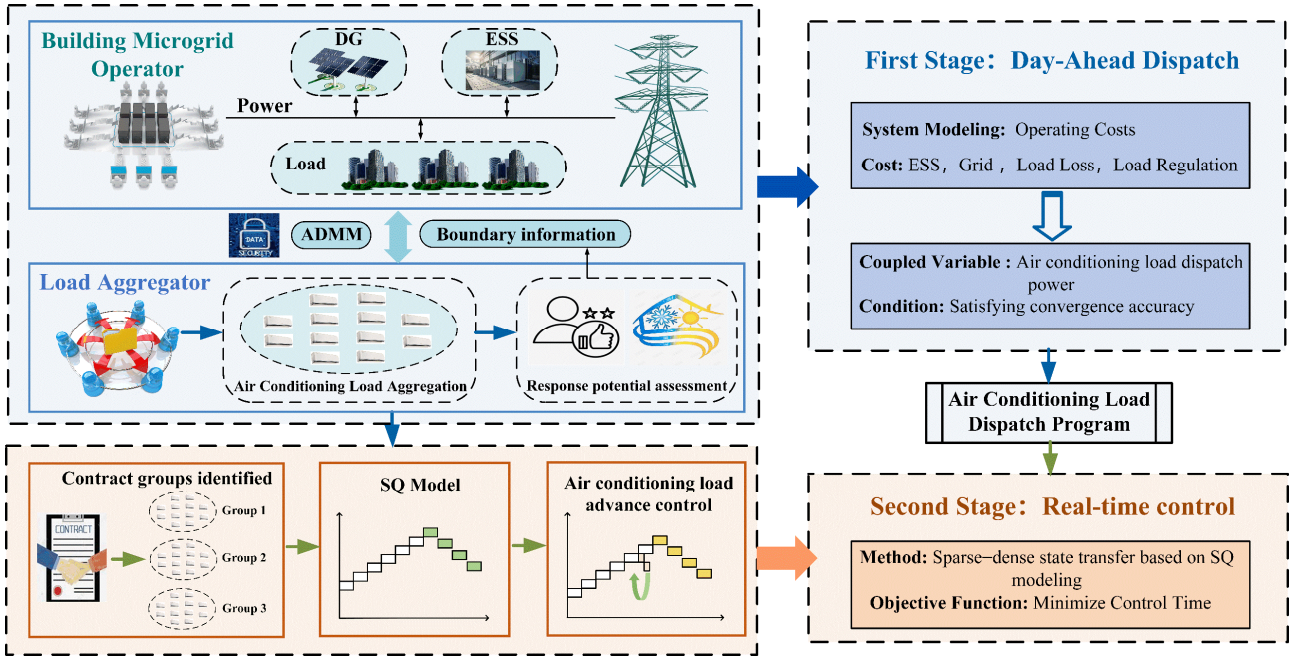

Figure 1. Day-ahead and real-time aggregation and control framework for air conditioning loads in integrated BMG systems.

2.2. Approximate Aggregation Model of Air Conditioning Loads

2.2.1. Single-Zone RC Thermal Model for Buildings

To simplify the modeling process and improve the computational efficiency of large-scale aggregated scheduling, this paper adopts a single-zone RC thermal model to characterize the thermal dynamics of user buildings. The model assumes that the air conditioner regulates only the temperature of the primary occupied room, while heat transfer through the roof, floor, and adjacent rooms is neglected. The single-zone RC model represents an independently controlled zone rather than assuming a uniform temperature for the entire building. A typical single-zone RC thermal model for buildings is illustrated in Figure 2, where the walls, indoor, and outdoor environments are represented as network nodes. The thermal capacitance effects caused by wall thickness and indoor space are denoted by C_w and C_{in}, respectively, with the node temperatures serving as the state variables. It is important to note that heat exchange between internal rooms in a building is mutual. Therefore, when aggregating the heating/cooling demand for an entire building, the internal heat exchange process can be neglected for simplification.

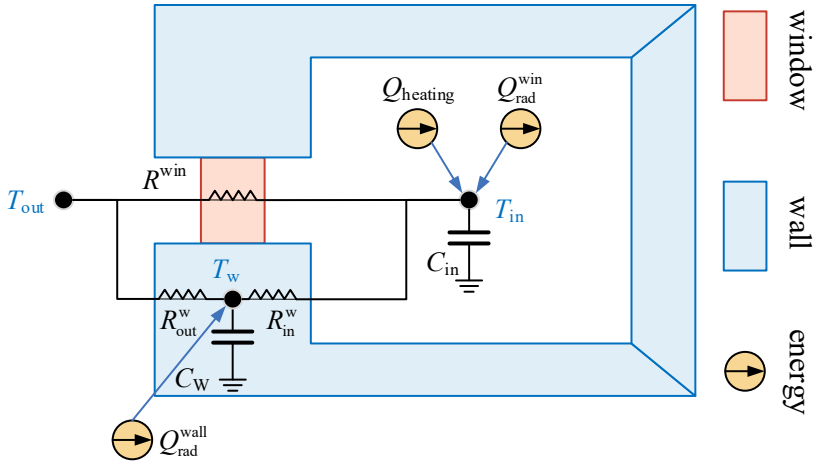

Figure 2. Single-zone RC thermal model for buildings.

The wall thermal balance constraint for a single-zone user is expressed as

$$C_w \frac{dT_{\text{wall}}}{dt} = \frac{T_{\text{in}} - T_{\text{wall}}}{R_{\text{in}}^{\text{wall}}} + \frac{T_{\text{out}} - T_{\text{wall}}}{R_{\text{out}}^{\text{wall}}} + \gamma A Q_{rad}^{\text{wall}} \tag{1}$$

where T_{wall}, T_{in} and T_{out} represent the temperatures of the wall, indoor, and outdoor nodes, respectively. $R_{\text{in}}^{\text{wall}}$ and $R_{\text{out}}^{\text{wall}}$ denote the thermal resistances of the wall's inner and outer layers, which are connected to the indoor and outdoor nodes, respectively. γ represents the solar absorptivity of the building wall, which depends on its orientation. A denotes the external surface area of the building wall (excluding window areas), and Q_{rad}^{wall} is the solar irradiance corresponding to that wall surface.

The indoor thermal balance constraint for a single-zone user is expressed as

$$\begin{aligned} C_{\text{in}} \tfrac{dT_{\text{in}}}{dt} = \tfrac{T_{\text{wall}} - T_{\text{in}}}{R_{\text{in}}^{\text{wall}}} + \xi_{\text{in}} \tfrac{T_{\text{out}} - T_{\text{in}}}{R_{w,\text{in}}} + \\ \xi_{\text{in}} \gamma^{w} A^{w,\text{in}} Q_{\text{rad}}^{w,\text{in}} + m_t \beta_{\text{sea}} Q_{\text{int}} \end{aligned} \tag{2}$$

$$m_t = \begin{cases} 0, & T_{\text{in}} \le T_{\text{set}} - 0.5\delta \\ 1, & T_{\text{in}} \ge T_{\text{set}} + 0.5\delta \\ m_{t-\varepsilon} & \text{other} \end{cases} \tag{3}$$

where ξ_{in} is the window presence coefficient (1 if a window is present, otherwise 0); $R_{w,\text{in}}$ represents the thermal resistance of the window; γ^{w} is the solar transmittance of the window; $A^{w,\text{in}}$ denotes the window area; $Q_{\text{rad}}^{w,\text{in}}$ represents the solar irradiance corresponding to the window; m_t is the on/off status of the air conditioning load, as defined in Equation (3); β_{sea} is the seasonal coefficient, set to -1 in summer and 1 in winter—this study primarily considers summer conditions, so $\beta_{\text{sea}} = -1$; Q_{int} represents the cooling (or heating) power of the air conditioning unit, which is related to the rated power by $P_{\text{int}} = Q_{\text{int}}/\eta$; η is the energy efficiency ratio; T_{set} denotes the air conditioner temperature setpoint, which is set to 26 °C; δ denotes the deadband of the air conditioning control, with a value of 1 °C; and ε denotes the simulation time step.

Solving for T_{in} using the system of ordinary differential equations derived from Equations (1) and (2) leads to a second-order nonhomogeneous differential equation with constant coefficients. This introduces two eigenvalues, making it difficult to directly determine the on/off duration of temperature-controlled loads. This paper assumes that T_{wall} can be linearized and rewrites it as a function of the indoor and outdoor temperatures at the same time instant. This approximation is mainly applicable to scenarios where the outdoor temperature and solar irradiance vary slowly within a single control cycle, and where the thermal inertia of the building envelope makes the temporal variation of T_{wall} relatively smooth:

$$T_{\text{wall}} = A_1 T_{\text{in}} + A_2 T_{\text{out}} + A_3 \tag{4}$$

$$\begin{cases} A_1 = \frac{1}{2} \frac{C_w R_{\text{in}}^{\text{wall}} R_{\text{out}}^{\text{wall}} + 2R_{\text{out}}^{\text{wall}}}{C_w R_{\text{in}}^{\text{wall}} R_{\text{out}}^{\text{wall}} + R_{\text{out}}^{\text{wall}} + R_{\text{in}}^{\text{wall}}} \\ A_2 = \frac{1}{2} \frac{C_w R_{\text{in}}^{\text{wall}} R_{\text{out}}^{\text{wall}} + 2R_{\text{in}}^{\text{wall}}}{C_w R_{\text{in}}^{\text{wall}} R_{\text{out}}^{\text{wall}} + R_{\text{out}}^{\text{wall}} + R_{\text{in}}^{\text{wall}}} \\ A_3 = \frac{\gamma A Q_{\text{rad}}^{\text{wall}} R_{\text{in}}^{\text{wall}} R_{\text{out}}^{\text{wall}}}{C_w R_{\text{in}}^{\text{wall}} R_{\text{out}}^{\text{wall}} + R_{\text{out}}^{\text{wall}} + R_{\text{in}}^{\text{wall}}} \end{cases} \tag{5}$$

By substituting Equation (5) into Equation (2), Equation (2) can be rewritten as a first-order nonhomogeneous linear differential Equation with T_{in} as the only state variable:

$$\frac{dT_{\text{in}}}{dt} = \begin{cases} A_4 T_{\text{in}} + A_5 T_{\text{out}} + A_6 & m_t = 1 \\ A_4 T_{\text{in}} + A_5 T_{\text{out}} + A_7 & m_t = 0 \end{cases} \tag{6}$$

$$\begin{cases} A_4 = \frac{(A_1-1)R_{w,in}-\xi_{in}R_{\text{in}}^{\text{wall}}}{C_{in}R_{\text{in}}^{\text{wall}}R_{w,in}} \\ A_5 = \frac{A_2R_{w,in}+\xi_{in}R_{\text{in}}^{\text{wall}}}{C_{in}R_{\text{in}}^{\text{wall}}R_{w,in}} \\ A_6 = \frac{A_3+(\xi_{in}\gamma^w A^{w,in}Q_{rad}^{w,in}+\beta_{sea}Q_{\text{int}})R_{\text{in}}^{\text{wall}}}{C_{in}R_{\text{in}}^{\text{wall}}} \\ A_7 = \frac{A_3+\xi_{in}\gamma^w A^{w,in}Q_{rad}^{w,in}R_{\text{in}}^{\text{wall}}}{C_{in}R_{\text{in}}^{\text{wall}}} \end{cases} \tag{7}$$

By solving Equation (7), the single-cycle ON duration t_o and OFF duration t_c of the thermostatically controlled load can be obtained, and their sum yields the total ON/OFF duration of one control cycle:

$$\begin{cases} t_o = -\frac{1}{A_4}\ln(\frac{T_{\text{set}}+B_1/A_4+0.5\delta}{T_{\text{set}}+B_1/A_4-0.5\delta}) \\ t_c = -\frac{1}{A_4}\ln(\frac{T_{\text{set}}+B_2/A_4-0.5\delta}{T_{\text{set}}+B_2/A_4+0.5\delta}) \\ B_1 = A_5T_{\text{out}}+A_6 \\ B_2 = A_5T_{\text{out}}+A_7 \end{cases} \tag{8}$$

2.2.2. Air Conditioning Load Group Model

The power consumption of a single air conditioner can be modeled based on its own characteristics; however, for the LA and BMO, the primary focus is on the aggregated air conditioning power of the load cluster.

$$P_{\text{agg}}^t = \sum_{i=1}^{N} P_{\text{int}}p_{\text{on},i} \tag{9}$$

where P_{agg}^t represents the aggregated power of the air conditioning load cluster; $p_{\text{on},i}$ denotes the probability of the i-th air conditioning load being in the ON state; and N is the total number of air conditioning loads in the cluster.

For a single air conditioning unit, its average power consumption is solely determined by the duty cycle of its ON state. Therefore, the probability of being in the ON state is denoted as $p_{\text{on},i}$, and it is calculated as follows:

$$p_{\text{on},i} = \frac{t_o}{t_o+t_c} \tag{10}$$

Substituting Equation (4) into Equation (6) and applying inequality transformations, we obtain

$$\begin{aligned} \frac{C_{\text{in}}A_4(B_2/A_4+T_{\text{set}}+0.5\delta)}{\eta_i P_{\text{int},i}} &\le P_{\text{on},i} \\ \frac{C_{\text{in}}A_4(B_2/A_4+T_{\text{set}}-0.5\delta)}{\eta_i P_{\text{int},i}} &\ge P_{\text{on},i} \end{aligned} \tag{11}$$

From the above Equation (11), the upper and lower bounds of the approximate aggregated power for an N-load cluster can be derived as

$$\begin{cases} P_{\text{agg,up}} = \sum\limits_{i=1}^{N} \dfrac{C_{\text{in}}A_4(B_2/A_4+T_{\text{set}}-0.5\delta)}{\eta_i} \\ P_{\text{agg,down}} = \sum\limits_{i=1}^{N} \dfrac{C_{\text{in}}A_4(B_2/A_4+T_{\text{set}}+0.5\delta)}{\eta_i} \end{cases} \tag{12}$$

where $P_{\text{agg,up}}$ represents the upper bound of the aggregated-air conditioning load power, and $P_{\text{agg,down}}$ represents the lower bound of the aggregated-air conditioning load power cluster.

Therefore, the estimated aggregated power of the load cluster can be represented by any value within the interval $\left[P_{\text{agg,down}}, P_{\text{agg,up}}\right]$.

$$\widetilde{P}_{\text{agg}} = \alpha P_{\text{agg,down}} + (1-\alpha) P_{\text{agg,up}} \qquad \alpha \in [0,1] \tag{13}$$

2.3. Multi-Factor Air Conditioning Load Response-Potential Model

Currently, most definitions of demand-response potential focus on the ability of the load power to increase or decrease during a demand-response event. To further explore the response potential of air conditioning loads, this study comprehensively considers user comfort and willingness to participate as key factors in evaluating air conditioning load response potential.

(1) User Comfort Level

To more comprehensively characterize user comfort perception, the Predicted Mean Vote (PMV) index, formulated based on the international standard ISO 7730 [30], is introduced to quantify users' thermal comfort perceptions. It is assumed that, except for air temperature T_{in}, all other parameters are given as fixed values. To highlight the relationship between the PMV index and indoor temperature, a simplified form of the PMV equation is derived as follows:

$$I_{\text{PMV},t} = 2.43 - \frac{3.76(T_{\text{sk}} - T_{\text{in}})}{M(I_{\text{cl}} + 1)} \tag{14}$$

where $I_{\text{PMV},t}$ is the PMV value of the indoor user at time t; T_{sk} represents the average skin temperature when the human body perceives comfort, typically set to 34 °C; M denotes the metabolic rate of the human body, typically set to 1 met; and I_{cl} is the thermal resistance of clothing, typically set to 0.5 clo. Thus, the relationship between indoor temperature and PMV can be expressed as

$$T_{\text{in},t} = T_{\text{sk}} - \frac{(2.43 - I_{\text{PMV},t})(I_{\text{cl}} + 0.1)M}{3.76} \tag{15}$$

The PMV comfort index is a comprehensive metric that integrates multiple factors affecting human comfort, including air temperature, humidity, airflow velocity, clothing insulation, and physical activity level. It quantifies human comfort on a standardized scale within the range of $[-1, 1]$. According to its definition, when $I_{\text{PMV}} = 0$, users experience optimal comfort. However, as I_{PMV} deviates further from zero, the perceived comfort level decreases. By substituting $I_{\text{PMV}} = 1, -1$ into Equation (15), the user's comfort temperature range $[T_{\text{in},t}^{\text{down0}}, T_{\text{in},t}^{\text{up0}}]$ can be obtained.

(2) User Willingness Degree

User willingness degree is assessed by comparing electricity costs with psychological expectations. When the electricity price exceeds the baseline price, users perceive the cost as higher than expected, increasing their willingness to participate in demand response. Consequently, they lower their thermal comfort requirements and expand the acceptable temperature range. Conversely, when the electricity price falls below the baseline price, willingness to participate decreases, and the acceptable temperature range narrows.

Willingness reflects users' sensitivity to electricity price variations and is influenced by factors such as income level, educational attainment, and age. To ensure engineering implementability and reproducibility, this study adopts a relatively simplified set of influencing factors in the user willingness model to capture how user heterogeneity affects participation in demand response. Meanwhile, the corresponding coefficient values are specified based on publicly available census data. Typically, users with lower income, higher education levels, and younger demographics are more inclined to participate in

demand response programs. To quantify these influences, the education level coefficient φ_1, household income coefficient φ_2, and average age coefficient φ_3 are introduced. Together, they determine the subjective response coefficient φ, which measures users' price sensitivity and participation willingness $\mu_{i,t}$ [31].

$$\mu_{i,t} = \varphi(e^{\frac{p_{real}}{p_{\max}}-1} - e^{\frac{p_{base}}{p_{\max}}-1}) \tag{16}$$

$$\varphi = \frac{\varphi_1\varphi_2\varphi_3}{\max(\varphi_1, \varphi_2, \varphi_3)} \tag{17}$$

$$\varphi_1 = \begin{cases} a_1, & 0 \le edu \le \omega_1 \\ a_2, & \omega_1 \le edu \le \omega_2 \\ a_3, & \omega_2 \le edu \le \omega_3 \end{cases} \tag{18}$$

$$\varphi_2 = \begin{cases} e^{-I}, & 0 \le I \le \omega_4 \\ e^{-\omega_4}, & I \ge \omega_4 \end{cases} \tag{19}$$

$$\varphi_3 = a_4 e^{-\frac{(A_{age}-\omega_5)}{2}} \tag{20}$$

where $0 \le a_1 < a_2 < a_3 \le 1$, $0 \le a_4 \le 1$, $\omega_1, \omega_2, \omega_3$ is the user's education level, increasing from high to low; ω_4 is the threshold of user willingness influenced by household income; ω_5 denotes the average age of the user group; edu is the user's education level; I is household income; and A_{age} is the average age of household users.

From the above equation, it is clear that the willingness factor $\mu_{i,t}$ represents the willingness of the ith user to participate in a demand-response event at time t. When $\mu_{i,t}$ is positive, it indicates that the user tends to participate more actively in demand response under a price level higher than the baseline and is willing to relax comfort constraints to some extent; when $\mu_{i,t}$ is negative, it indicates that the user tends to maintain the original comfort level under a price level lower than the baseline and is less inclined to participate. The strength of this tendency is reflected by the absolute value of $\mu_{i,t}$, with a larger magnitude indicating a stronger propensity.

By considering the user's willingness factors, the temperature constraint range originally determined by the user comfort model can dynamically change. The temperature variation formula is as follows:

$$\Delta T_{i,t} = \mu_{i,t}(T_{\text{in},t}^{\text{up0}} - T_{\text{in},t}^{\text{down0}}) \tag{21}$$

where $\Delta T_{i,t}$ is the temperature adjustment variation in the ith air conditioning device at time t, considering user willingness factors.

Thus, after considering user willingness, the temperature constraint range becomes $[T_{\text{in},t}^{\text{down}}, T_{\text{in},t}^{\text{up}}]$, which is calculated as follows:

$$T_{\text{in},t}^{\text{up}} = T_{\text{in},t}^{\text{up0}} + \Delta T_{i,t} \tag{22}$$

$$T_{\text{in},t}^{\text{down}} = T_{\text{in},t}^{\text{down0}} - \Delta T_{i,t} \tag{23}$$

where $T_{\text{in},t}^{\text{down}}$ and $T_{\text{in},t}^{\text{up}}$ are the upper and lower temperature constraint limits, respectively, considering both user comfort and willingness.

If α is 0.5, the air conditioning cluster response power range is $\left[P_{ac,t}^{min}, P_{ac,t}^{max}\right]$. The formulas for the maximum response power, minimum response power, and response potential are as follows:

$$P_{ac,t}^{max} = \sum_{i=1}^{N} \frac{C_{in} A_4 (B_2/A_4 + T_{in,t}^{down})}{\eta_i} \tag{24}$$

$$P_{ac,t}^{min} = \sum_{i=1}^{N} \frac{C_{in} A_4 (B_2/A_4 + T_{in,t}^{up})}{\eta_i} \tag{25}$$

$$\Delta P_{ac,t} = \sum_{i=1}^{N} \frac{C_{in} A_4 (T_{in,t}^{down} - T_{in,t}^{up})}{\eta_i} \tag{26}$$

where $P_{ac,t}^{min}$ and $P_{ac,t}^{max}$ are the maximum and minimum response power values of the air conditioning cluster, respectively, corresponding to the temperature constraint limits determined by considering both user comfort and willingness; $\Delta P_{ac,t}$ is the response potential of the air conditioning cluster at this time.

2.4. Day-Ahead Distributed-Scheduling Model for BMO-LA Considering Response Potential

The BMO and LA are typically separate entities. To prevent individual users from directly interacting with the BMO, which could lead to the exposure of user energy consumption data, air conditioning users do not share their device information with the BMO for privacy protection. Therefore, this study develops a day-ahead distributed-scheduling model from the perspectives of the BMO and LA, considering the potential of air conditioning load control.

2.4.1. Objective Function

The power output facilities in residential buildings mainly include energy storage systems and rooftop PV systems. To fully highlight the peak-shaving and valley-filling advantages of air conditioning loads, this section assumes that the operating cost of renewable energy generation is zero. Thus, the total operating cost consists of the following four components: (i) the cost of purchasing electricity from the main grid, (ii) the charging and discharging cost of energy storage systems, (iii) compensation cost for air conditioning loads, (iv) the penalty cost for load shedding. The specific formulation is given in Equation (27).

$$\min f = \sum_{t=1}^{T} C_{grid,t} P_{grid,t} + C_{ess} |P_{ess,t}| + C_{ac} P_{ac,t} + C_{loss} P_{loss,t} \tag{27}$$

where $C_{grid,t}$ and $P_{grid,t}$ represent the electricity purchase price and purchased electricity volume from the grid, respectively; C_{ess} and $P_{ess,t}$ denote the charging/discharging cost coefficient and charging/discharging power of the energy storage system, respectively; C_{ac} and $P_{ac,t}$ correspond to the compensation price per unit of electricity for air conditioning loads and the target power, respectively; and C_{loss} and $P_{loss,t}$ represent the penalty price for load shedding and the amount of shed load, respectively.

2.4.2. Constraints

(1) Power Balance Constraint

$$P_{grid,t} + P_{ess,t}^{D} + P_{PV,t} = P_{l,t} + P_{ess,t}^{C} - P_{ac,t} - P_{loss,t} \tag{28}$$

where $P^{C}_{\mathrm{ess},t}$ and $P^{D}_{\mathrm{ess},t}$ represent the charging and discharging power of the energy storage system, respectively; $P_{\mathrm{PV},t}$ denotes the predicted PV output; and $P_{l,t}$ represents the load demand at time t.

(2) Air Conditioning Load Response-Potential Constraint

$$P^{\min}_{\mathrm{ac},t} \le P_{\mathrm{ac},t} \le P^{\max}_{\mathrm{ac},t} \tag{29}$$

(3) PV Output Constraint

$$0 \le P_{\mathrm{PV},t} \le P^{\max}_{\mathrm{PV},t} \tag{30}$$

(4) Power Purchase Constraint

$$0 \le P_{\mathrm{grid},t} \le P_{\mathrm{grid,max}} \tag{31}$$

where $P_{\mathrm{grid,max}}$ represents the maximum allowable power purchase from the grid.

(5) Energy Storage Charging and Discharging Constraints

$$\begin{cases} 0 \le P^{D}_{\mathrm{ess},t} \le P^{D}_{\mathrm{ess,max}}\chi_{D,t} \\ 0 \le P^{C}_{\mathrm{ess},t} \le P^{C}_{\mathrm{ess,max}}\chi_{C,t} \\ \chi_{D,t} + \chi_{C,t} \le 1 \\ S_{\mathrm{ess},t} = S_{\mathrm{ess},t-1} + P^{C}_{\mathrm{ess},t}\eta^{C}_{\mathrm{ess}} - P^{D}_{\mathrm{ess},t}\eta^{D}_{\mathrm{ess}} \\ S^{\min}_{\mathrm{ess}} \le S_{\mathrm{ess},t} \le S^{\max}_{\mathrm{ess}} \end{cases} \tag{32}$$

where $P^{C}_{\mathrm{ess,max}}$ and $P^{D}_{\mathrm{ess,max}}$ represent the maximum charging and discharging power of the energy storage system, respectively; $\chi_{C,t}$ and $\chi_{D,t}$ are binary variables indicating the charging and discharging states of the energy storage system; η^{C}_{ess} and η^{D}_{ess} denote the charging and discharging efficiency of the energy storage system; and $S^{\min}_{\mathrm{ess}}$ and $S^{\max}_{\mathrm{ess}}$ represent the storage capacity limits of the energy storage system.

2.4.3. Distributed Solution Based on ADMM Algorithm

Equations (27)–(32) constitute a centralized optimization scheduling model. However, when users have privacy protection requirements, integrating load consumption optimization and building energy supply scheduling into a single unified model is impractical. To address this, this study adopts the ADMM algorithm, leveraging its advantages in distributed solving. ADMM effectively protects user privacy while also handling complex constraints efficiently by introducing Lagrange multipliers, ensuring good algorithm convergence. Thus, the centralized optimization problem in Equation (27) is decomposed into two subproblems: the BMO optimization scheduling subproblem and the central air conditioning scheduling subproblem. If more complex stochastic uncertainties are considered, such as random disturbances in real-time loads, stochastic-ADMM and related approaches could be explored.

$$\begin{aligned} \min f_1 &= \sum_{t=1}^{T} C_{\mathrm{grid},t}P_{\mathrm{grid},t} + C_{\mathrm{ess},t}|P_{\mathrm{ess},t}| + C_{\mathrm{loss},t}P_{\mathrm{loss},t} \\ \min f_2 &= \sum_{t=1}^{T} C_{\mathrm{ac},t}P_{\mathrm{ac},t} \end{aligned} \tag{33}$$

By introducing the Lagrange multiplier λ_ρ and the penalty term ρ_P, the objective function is expressed as

$$\begin{aligned}&\min S_1 = \\ &\sum_{t=1}^{T} C_{\text{grid},t}P_{\text{grid},t} + C_{\text{ess},t}|P_{\text{ess},t}| + C_{\text{loss},t}P_{\text{loss},t} + \lambda_\rho(P_{\text{int},t} - \overline{P}_{\text{int},t}) + \frac{\rho_P}{2}\left\|P_{\text{int},t} - \overline{P}_{\text{int},t}\right\|_2^2\end{aligned} \tag{34}$$

$$\min S_2 = \sum_{t=1}^{T} C_{\text{ac},t}P_{\text{ac},t} + \lambda_\rho(P_{\text{ac},t} - \overline{P}_{\text{int},t}) + \frac{\rho_P}{2}\left\|P_{\text{ac},t} - \overline{P}_{\text{int},t}\right\|_2^2 \tag{35}$$

$$\overline{P}_{\text{int},t} = \frac{P_{\text{int},t} + P_{\text{ac},t}}{2} \tag{36}$$

where $\overline{P}_{\text{int},t}$ represents the average value of the coupling variable between the two subproblems.

The specific steps of the algorithm are illustrated in Figure 3:

(1) Parameter Initialization: Set the iteration index $r = 0$ and the convergence precision $\varepsilon = 10^{-3}$, initialize the iteration count to 0, and initialize the coupling variable $P^0_{\text{int},t} = P^0_{\text{ac},t} = 0$, the Lagrange multiplier $\lambda_\rho = 0$, and the penalty factor $\rho_P = 0$.

(2) Boundary Information Sharing: The BMO entity and LA entity share their respective coupling variable information, forming a synchronous ADMM. The solution formulation is given in Equation (36).

(3) Solving the Scheduling Subproblems: For the BMO, receive the scheduled air conditioning load power $P_{ac,t}$ from the LA, solve the scheduling subproblem S_1, and update the planned scheduling power $P^{r+1}_{\text{int},t}$ for air conditioning loads in the BMG. For the LA, receive the scheduled air conditioning load power $P^{r+1}_{\text{int},t}$ from the BMO, solve the scheduling subproblem S_2, and determine the planned response amount $P^{r+1}_{ac,t}$ for the LA. Update the coupling variable $\overline{P}^{r+1}_{\text{int},t}$ using Equation (36).

(4) Updating the Lagrange Multiplier and Iteration Count: Update the Lagrange multiplier according to Equation (37).

$$\lambda^{\text{r}+1}_{p,t} = \lambda^{\text{r}}_{p,t} + \rho^{r+1}_p(P^{r+1}_{\text{int},t} - \overline{P}^{r+1}_{\text{int},t}) \tag{37}$$

Update the algorithm iteration count by incrementing it by one.

$$r = r + 1 \tag{38}$$

(5) Determine the algorithm convergence condition. If the termination condition in Equation (39) is satisfied, the iteration process terminates; otherwise, return to Step 2 and repeat the computation until either the convergence condition is satisfied or the maximum iteration count is reached.

$$\begin{cases} \sum_{t=1}^{T} \left\|P_{\text{int},t} - \overline{P}_{\text{int},t}\right\|_2^2 < \varepsilon \\ \text{or} \quad r > r_{\max} \end{cases} \tag{39}$$

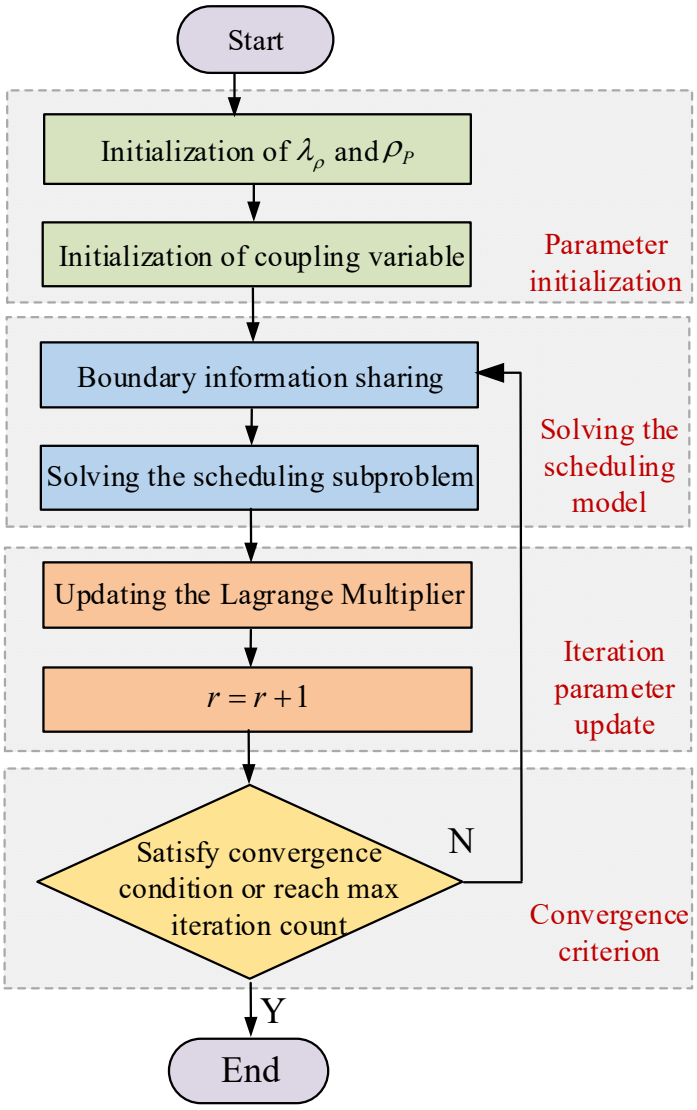

Figure 3. ADMM algorithm flowchart.

2.5. SQ-Based Pre-Emptive Control Strategy for Air Conditioning Load

Due to the non-uniform initial indoor-temperature distribution among users, the actual air conditioning load response may deviate from the expected value, thereby affecting the execution of the scheduling plan. To address this issue, this paper proposes a pre-regulation strategy for air conditioning loads based on a state queue model, aiming to achieve balanced load distribution through refined management.

The state queue model refers to the linear discretization of air conditioning operating states into several discrete states within a complete control cycle, with each state corresponding to a specific temperature level. As shown in Equation (8), the durations of the air conditioner being in the ON and OFF states during the control cycle are denoted by t_o and t_c, respectively. The fundamental expression of the model is given in Equation (40):

$$T_{\text{in},t+1} = \begin{cases} T_{\text{in,t}} + (T_{\max} - T_{\min})\Delta t / t_c & m_t = 0 \\ T_{\text{in,t}} - (T_{\max} - T_{\min})\Delta t / t_o & m_t = 1 \end{cases} \tag{40}$$

To account for the impact of parameter heterogeneity on control performance, K-means clustering is applied to the temperature variation parameters derived from the ON/OFF cycles of air conditioning loads. The main reason for choosing K-means is that it has a

low computational cost, requires minimal distributional assumptions, and involves fewer hyperparameters, enabling stable user grouping within the real-time control loop and providing interpretable cluster centroids for setting group-level control parameters in the subsequent SQ-based scheme. The cluster centroids are used as the basis for grouping, and it is assumed that air conditioners within the same group share homogeneous parameters. Control tasks are then allocated according to the aggregated power of each group. For each air conditioning load within a cluster, N distinct temperature ranges and corresponding initial temperatures are defined. Based on the temperature range determined during potential evaluation, contract groups are formed. The upper and lower bounds of the temperature ranges for each contract group increase in increments of 0.5 °C. Each load within a group signs a day-ahead response contract with the load aggregator, selecting from K available temperature intervals. When dispatching control tasks, the load aggregator assigns regulation tasks to each contract group based on the control capacity of that group. The control capacity of an individual load is calculated using Equation (41). Based on the air conditioning parameters and the number of users n within each contract group, the load aggregator can compute the total aggregated control capacity of the group, as shown in Equation (42).

$$P_{\text{control},i,t} = \frac{t_{c,i}}{t_{o,i} + t_{c,i}} P_{\text{int},i,t} \tag{41}$$

$$P_{\text{control},t} = \sum_{j=1}^{n} P_{\text{control,i},t} \tag{42}$$

After assigning the dispatch tasks to each contract group, the number of loads $n_{\text{close},k}$ that need to be controlled within each contract group can be determined based on Equations (8) and (42).

Using the state queue model, the contract groups are divided into M temperature intervals, where the number of air conditioning loads in the m-th interval is denoted as $n_{\text{on},m}$. Due to the uneven distribution of users' initial indoor temperatures, when applying the state queue model, boundary intervals may suffer from low load density, making it difficult to ensure a uniform number of responsive loads across all temperature intervals, which may lead to power fluctuations. To address this issue, each contract group is divided into M temperature intervals, where the number of air conditioning loads in the m-th temperature interval is denoted as $n_{\text{on},m}$. A load distribution standard value $\gamma = n_{\text{close},k}/M$ is defined to assess the sparsity of load distribution across temperature intervals. If $\gamma > n_{\text{on},m}$, it indicates that the air conditioning load in this temperature interval is sparse, and the number of sparse intervals is recorded as n_{sparse}. Conversely, if $\gamma < n_{\text{on},m}$, it indicates that the load distribution is dense. In the actual dispatch process, to mitigate the uneven load distribution in dense intervals, a pre-emptive control strategy is employed to transfer a portion of the loads from dense intervals to sparse intervals, thereby achieving refined load management.

The principle of the pre-regulation strategy is illustrated in Figure 4. Before the dispatch plan is issued, if temperature state 4 is sparsely populated while temperature state 5 is densely populated, a portion of the loads in state 5 are precooled, while the loads in state 4 continue to warm up as usual. When both sets of loads reach the same temperature, the loads from state 5 are switched off and transition to the same state as those in state 4, thereby completing the pre-shifting process.

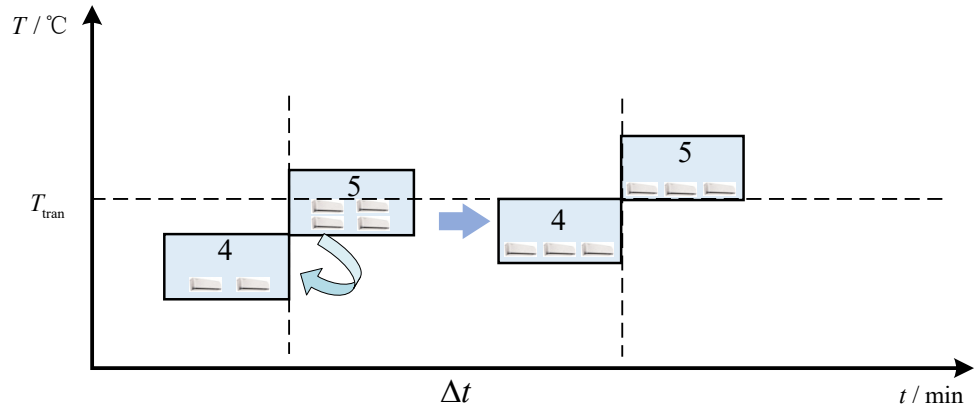

Figure 4. SQ-based pre-emptive control model.

The pre-shifting from densely populated states to sparsely populated states can be categorized into two scenarios: one involves lowering the temperature of the densely populated state to shift toward the sparse state, while the other involves raising the temperature for the same purpose. The corresponding operation time can be obtained by solving the system of equations formed by Equations (8) and (40):

(1) When $T_{\text{sparse,up},m} < T_{\text{dense,up},m_1}$: The transfer time is obtained by equating the time required for the sparse state to warm up to the intermediate temperature T_{tran,m_1} with the time required for the dense state to cool down to the same temperature T_{tran,m_1}.

$$\begin{cases} T_{\text{tran},m_1} = \frac{(B_1/A_4)T_{\text{sparse,up},m} - (B_2/A_4)T_{\text{dense,up},m_1}}{T_{\text{dense,up},m_1} - T_{\text{sparse,up},m} + (B_1 - B_2)/A_4} \\ \Delta t_{\text{d},m} = -\frac{1}{A_4}\ln\left(\frac{T_{\text{sparse,up},m} + B_2/A_4}{T_{\text{tran},m_1} + B_2/A_4}\right) \end{cases} \tag{43}$$

where $T_{\text{sparse,up},m}$ is the highest temperature of the queue module in the m-th sparse state, $T_{\text{dense,up},m_1}$ is the highest temperature of the queue module in the m_i-th dense state, and T_{tran,m_1} is the temperature after load transfer in the m_i-th state.

(2) When $T_{\text{sparse,up},m} > T_{\text{dense,up},m_1}$: At this point, the transfer time is divided into two stages. The first stage is the time required for the sparse state to shift to the upper temperature limit $T_{\text{max},k}$ of the contract group. The second stage is determined by equating the time for the dense state to warm up to temperature T_{tran,m_1} with the time for the sparse state to cool down to temperature T_{tran,m_1}.

$$T_{\text{later},m_1} = \frac{T_{\text{dense,up},m_1}(T_{\text{max},k} + B_2/A_4)}{T_{\text{sparse,up},m} + B_2/A_4} + \frac{B_2/A_4(T_{\text{max},k} - T_{\text{sparse,up},m})}{T_{\text{sparse,up},m} + B_2/A_4} \tag{44}$$

$$\begin{cases} T_{\text{tran},m_1} = \frac{(B_1/A_4)T_{\text{later},m_1} - (B_2/A_4)T_{\text{max},k}}{T_{\text{max},k} - T_{\text{later},m_1} + (B_1 - B_2)/A_4} \\ \Delta t_{\text{s},m} = -\frac{1}{A_4}\ln\left(\frac{T_{\text{sparse,up},m} + B_2/A_4}{T_{\text{max},k} + B_2/A_4}\right) - \frac{1}{A_4}\ln\left(\frac{T_{\text{max},k} + B_1/A_4}{T_{\text{tran},m_1} + B_1/A_4}\right) \end{cases} \tag{45}$$

where T_{later,m_1} is the transformed temperature of module m_i when transferring from a sparse state to the highest temperature, and $T_{\text{max},k}$ is the upper temperature limit of the k-th contract group.

To prevent air conditioning power drop, the number of loads in each temperature state of the state queue model should meet the required levels. Therefore, this paper establishes an objective function that minimizes the control time, formulated as follows:

$$\min T_i = \sum_{m=1}^{n_{\text{d}}} \Delta t_{\text{d},m} + \sum_{m=1}^{n_{\text{s}}} \Delta t_{\text{s},m} \tag{46}$$

The transfer constraints are defined as

$$\begin{cases} n_{\mathrm{d}} + n_{\mathrm{s}} = \sum_{m=1}^{n_{\mathrm{close},k}} \gamma - n_{\mathrm{min},m} \\ n_{\mathrm{on},m} - \gamma \geq 0 \end{cases} \tag{47}$$

where n_d is the number of loads transferred from the dense state group to the sparse state group when $T_{sparse,\mathrm{up,m}} < T_{\mathrm{dense,up,m}_1}$, $\Delta t_{\mathrm{d,m}}$ is the transfer time for each load in n_d, n_s is the number of loads transferred from the dense state group to the sparse state group when $T_{sparse,\mathrm{up,m}} > T_{\mathrm{dense,up,m}_1}$, $\Delta t_{\mathrm{s,m}}$ is the transfer time for each load in n_s, and $n_{\mathrm{min},m}$ is the number of loads in the k-th sparse state group.

3. Example Simulation

The experiments in this paper were all run on MATLAB software, with version R2024b.

3.1. Parameter Setting

In this case study, the BMG system consists of 6000 air conditioning units, with specific parameters listed in Table 1, where each parameter follows a uniform distribution within its respective range. The BMG system also includes PV generation, energy storage, and other functional devices, with their parameters and unit regulation costs provided in Table 2. The time-of-use electricity price is shown in Figure 5, while the PV output and load demand of the BMG system are illustrated in Figure 6.

Table 1. Building and air conditioning parameter settings.

Parameters	Value Range
$Q_{\mathrm{int}}/\mathrm{kW}$	[3, 4]
η_i	[2.5, 2.7]
$R^w_{\mathrm{in}}, R^w_{\mathrm{out}}/(^\circ\mathrm{C}\cdot\mathrm{kW}^{-1})$	[12.5, 13]
$R_{w,\mathrm{in}}/(^\circ\mathrm{C}\cdot\mathrm{kW}^{-1})$	[13.5, 14]
$C_w/(\mathrm{kW}\cdot\mathrm{h})\cdot{}^\circ\mathrm{C}^{-1}$	[2.5, 2.7]
$C_{\mathrm{in}}/(\mathrm{kW}\cdot\mathrm{h})\cdot{}^\circ\mathrm{C}^{-1}$	[0.7, 1]
$T_{\mathrm{set}}/^\circ\mathrm{C}$	[25, 27]
γ	[0.1, 0.15]
γ^w	[0.55, 0.6]
δ	1
ξ_{in}	1

Table 2. Building microgrid system parameters.

Parameters	Value Range
C_{ess}	0.1
C_{ac}	0.6
C_{loss}	2.5
$P_{\mathrm{grid,max}}$	3500
$P_{\mathrm{ess,min}}/P_{\mathrm{ess,max}}$	0/200
$S_{\mathrm{ess,min}}/S_{\mathrm{ess,max}}$	40/500
$S_{\mathrm{ess},0}$	150
$\eta^C_{\mathrm{ess}}/\eta^D_{\mathrm{ess}}$	0.96

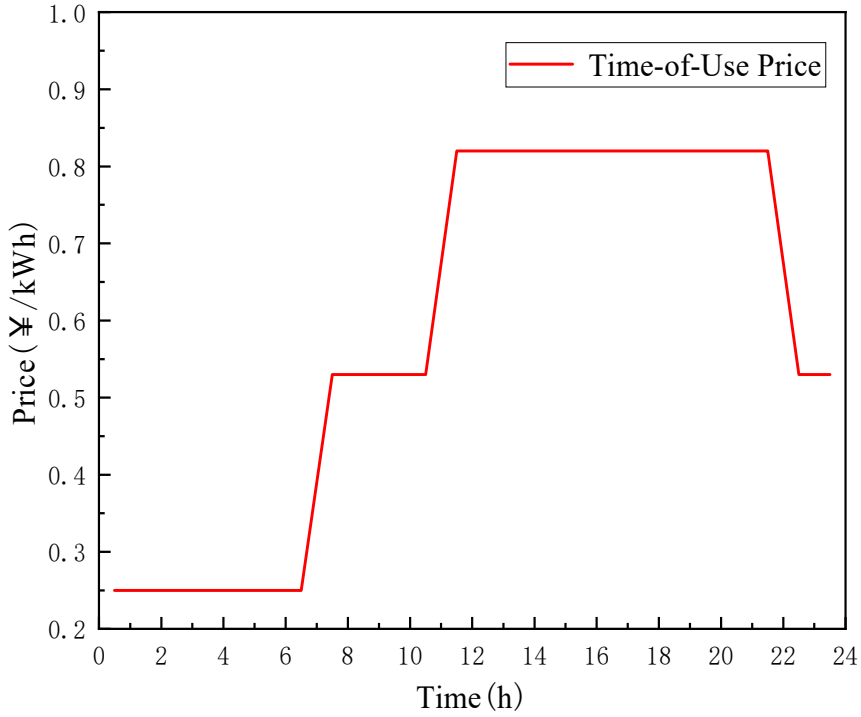

Figure 5. Time-of-use electricity price settings.

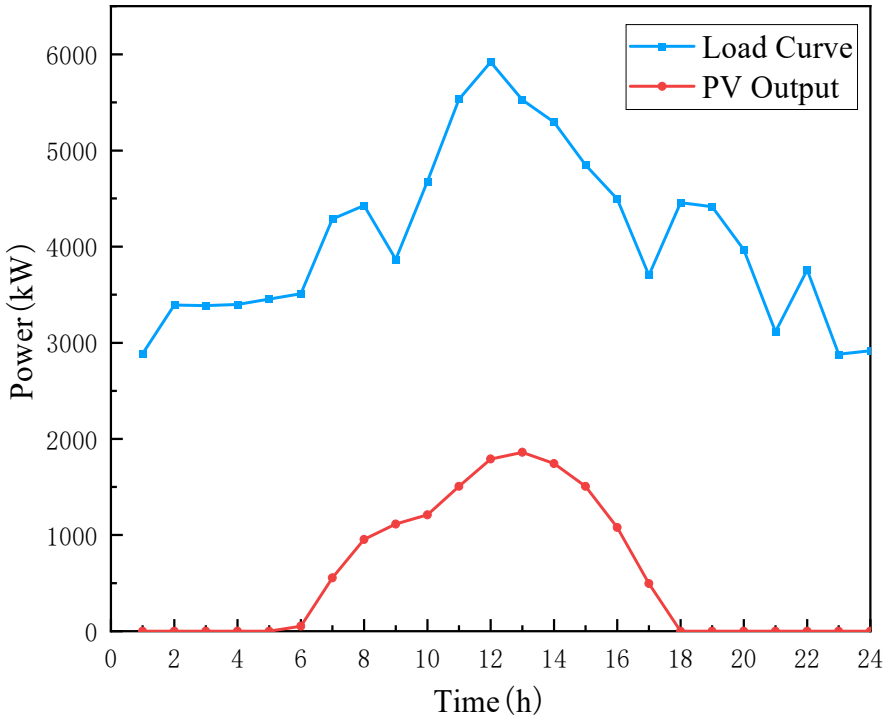

Figure 6. Building microgrid system load and PV data.

3.2. Validation of the Approximate Aggregation Model for Air Conditioning Loads

In this study, 6000 air conditioning units are simulated using the parameters set in Table 1, with Monte Carlo simulation results serving as the reference for actual power consumption comparison. The initial ON/OFF states of air conditioners are assumed to be randomly assigned. The aggregated air conditioning load power is analyzed under conditions of 34 °C temperature and 100% solar irradiance during 11:00–15:00. The simulation results are presented in Figure 7.

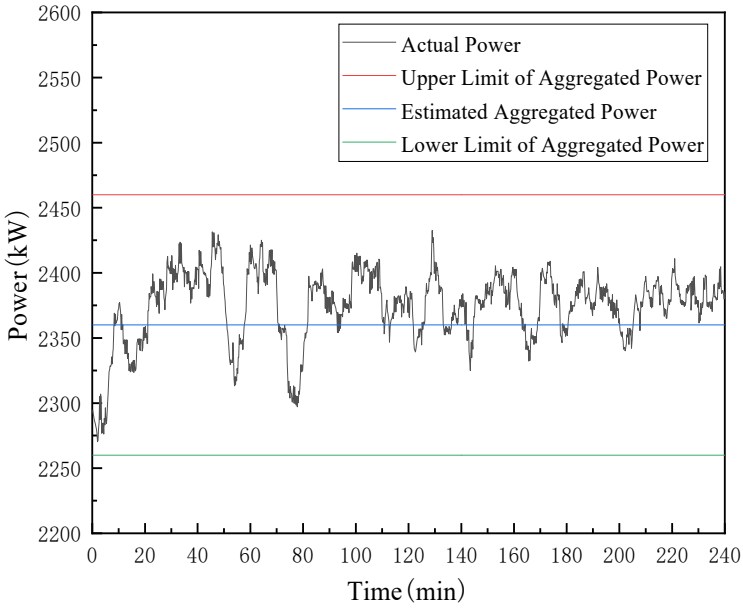

Figure 7. Estimated aggregated power of air conditioning loads and its upper and lower bounds.

From Figure 7, it can be observed that at 34 °C, the aggregated air conditioning load power of 6000 units stabilizes within the range of 2260–2460 kW. According to the proposed formula in this study, when $\alpha = 0.5$, the estimated aggregated power is 2361.3 kW. The estimated power bounds successfully encompass the actual power range, demonstrating a good approximation effect.

Figure 8 illustrates the aggregated power of building air conditioning loads under different solar irradiance levels and temperatures. The results indicate that as outdoor temperature increases and solar irradiance intensifies, the aggregated air conditioning power also rises. This is because the heat absorbed per unit of area per unit of time by the building increases with higher solar intensity and ambient temperature. Consequently, the time required for the indoor temperature to drop to the lower setpoint boundary increases, while the time for it to rise to the upper setpoint boundary decreases. As a result, the duty cycle of temperature-controlled devices increases, leading to a corresponding increase in the aggregated power consumption and maximum response power of building air conditioning loads.

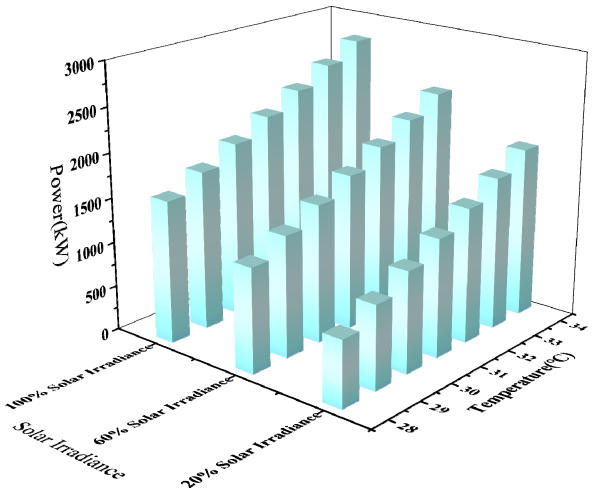

Figure 8. Aggregated power of building air conditioning loads under different light intensities and temperatures.

3.3. Simulation Analysis of Load Response Potential

To reasonably assess the response potential of the air conditioning load cluster and facilitate its effective participation in demand response, this study refers to the Seventh Population Census data published by the Anhui Provincial Bureau of Statistics, China. Using the flat-period electricity price in the time-of-use pricing scheme as the baseline price, the user willingness to participate in demand response at different time periods is obtained, as shown in Figure 9.

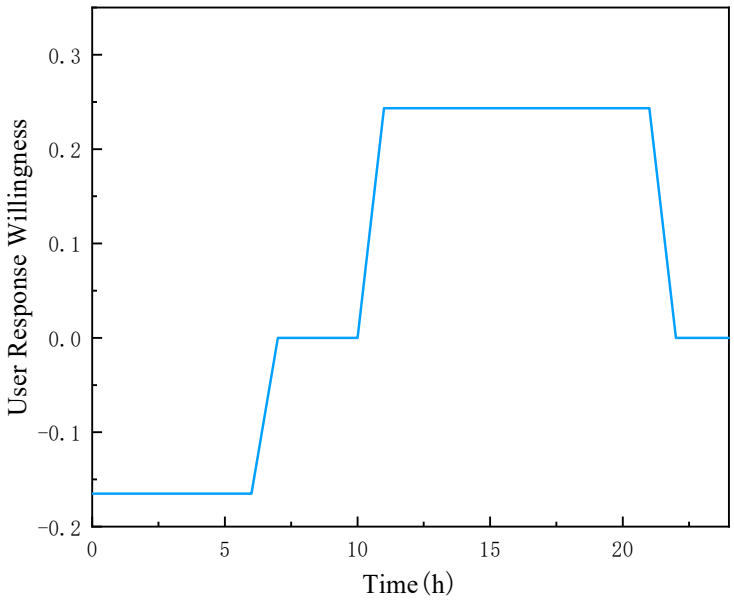

Figure 9. User response willingness.

From Figure 9, it can be observed that between 0:00 and 7:00, the electricity price is lower than the baseline price, resulting in a negative user willingness of −0.1653, indicating low participation willingness in demand response. Between 7:00 and 10:00, 16:00 and 18:00, and 21:00 and 24:00, the electricity price equals the baseline price, with a neutral willingness of 0, meaning users have no strong inclination to participate. Between 10:00 and 16:00 and 18:00 and 21:00, the electricity price is higher than the baseline price, leading to a positive user willingness of 0.2434, indicating a high participation willingness in demand response. Using Equations (22) and (23), the adjustable temperature range for users is calculated and presented in Figure 10.

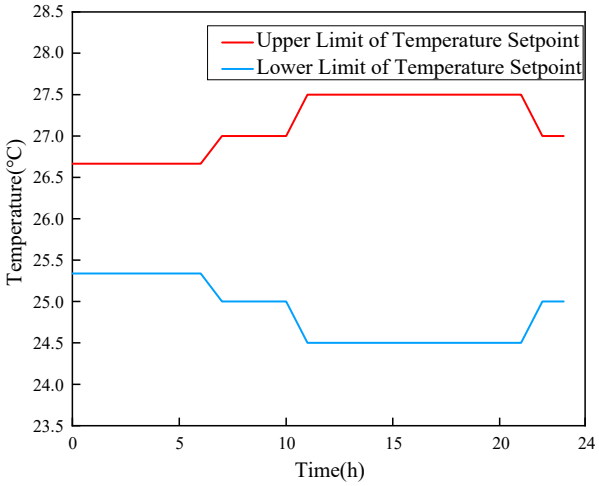

Figure 10. Temperature setpoint range based on user comfort and willingness.

Figure 10 illustrates the temperature setpoint range for air conditioning loads, evaluated based on user comfort and willingness indices. The red line represents the upper bound of the temperature setpoint range. The blue line represents the lower bound of the temperature setpoint range. During periods of low user willingness for demand response (negative willingness), users are reluctant to adjust their air conditioning temperature significantly. The adjustable range is 25.47–26.53 °C, which is slightly narrower than the original setpoint range. During periods when the electricity price equals the baseline price (neutral willingness), users hold a neutral stance toward demand-response participation, and the adjustable range remains unchanged from the original setpoint limits. During periods of high user willingness (positive willingness), users actively participate in demand response, and the adjustable temperature range expands to 24.5–27.5 °C.

The initial temperature setpoints of the air conditioning cluster are assumed to follow a uniform distribution between 25 °C and 27 °C, with an expected value of 26 °C. For the load reduction scenario, the evaluated response potential of the air conditioning cluster is shown in Figure 11.

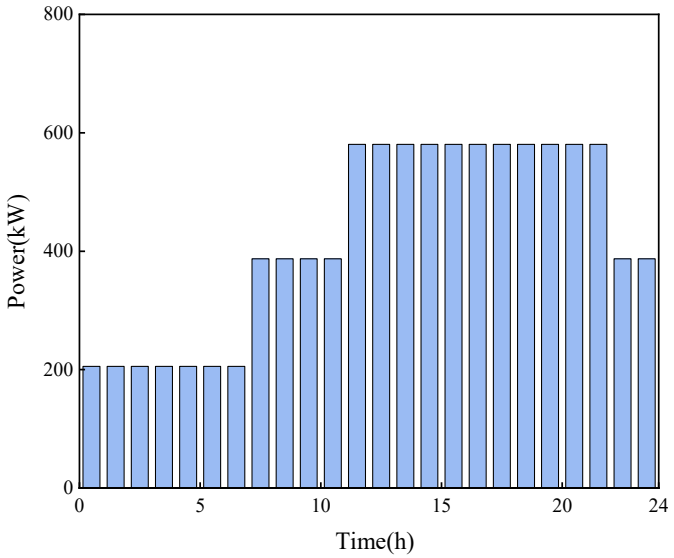

Figure 11. User response potential.

From Figure 11, it can be observed that during periods of low user willingness (negative willingness), the adjustable temperature range is narrow, resulting in a response potential of only 205.26 kW. During neutral willingness periods, where users hold a neutral stance on demand-response participation, the response potential increases to 387.02 kW. During periods of high user willingness (positive willingness), the adjustable temperature range expands further, leading to a response potential of 580.53 kW. These results demonstrate that the proposed evaluation model effectively assesses the aggregated response potential of air conditioning loads.

3.4. Simulation Analysis of the BMO-LA Day-Ahead Distributed-Scheduling Model

In this section, a simulation analysis of the BMO-LA day-ahead distributed-scheduling model is conducted. The initial values of the coupling variable and Lagrange multiplier are both set to 0. The initial value of the penalty parameter is set to 0.1. The maximum number of iterations is set to 50, and the convergence criterion is defined with the tolerances of both the primal and dual residuals set to 0.01.

Two scenarios are considered based on whether the response potential of air conditioning loads is taken into account:

- Scenario 1: Without considering the response potential of air conditioning loads.
- Scenario 2: Considering the response potential of air conditioning loads.

3.4.1. Scheduling Results Analysis

The hourly power scheduling results of Scenario 1 and Scenario 2 are shown in Figures 12 and 13, respectively. It can be observed that without considering the response-potential characteristics of air conditioning loads, load losses occur during peak periods from 11:00 to 14:00 and from 18:00 to 20:00 due to power purchase constraints from the grid. During the midday period, load losses are relatively small because of favorable photovoltaic output, whereas after 18:00, the photovoltaic output is almost zero, resulting in more significant load losses.

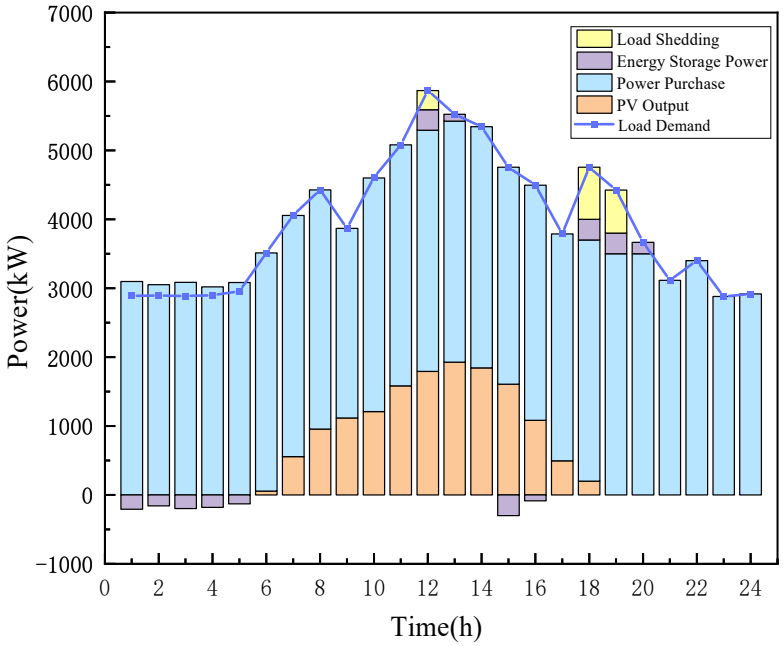

Figure 12. Scheduling results for Scenario 1.

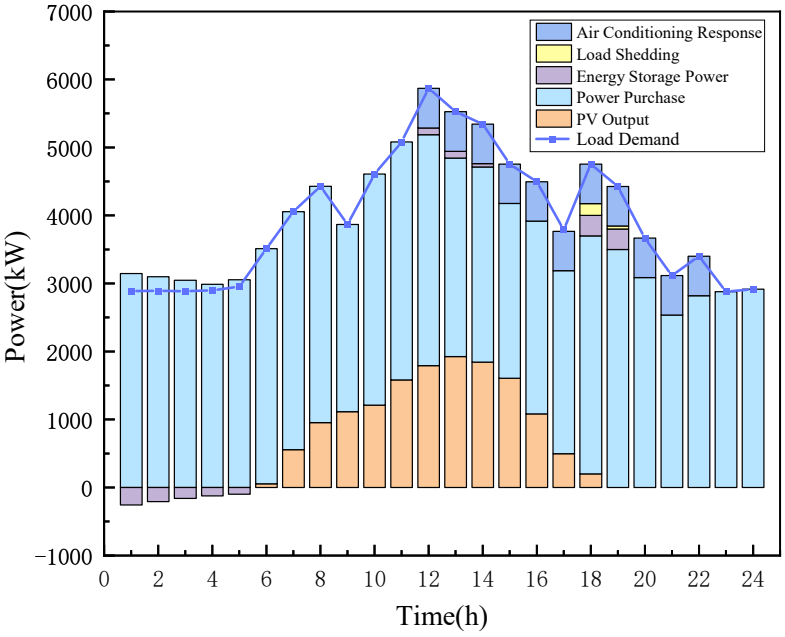

Figure 13. Scheduling results for Scenario 2.

In contrast, the scheduling results that consider the response potential of air conditioning loads demonstrate that the LA can reduce electricity consumption by compensating users, thereby balancing user comfort and willingness. During the midday peak from 11:00 to 14:00, the large air conditioning response potential combined with strong photovoltaic output eliminates load losses in the building microgrid system. Although photovoltaic output is absent between 18:00 and 20:00, the air conditioning response potential effectively reduces load losses during this period. Between 20:00 and 22:00, since the cost of load shifting is lower than the time-of-use electricity price, the air conditioning load response can reduce overall system operating costs. Figure 14 shows the algorithm iteration results, where convergence is achieved after 37 iterations, yielding a balanced solution.

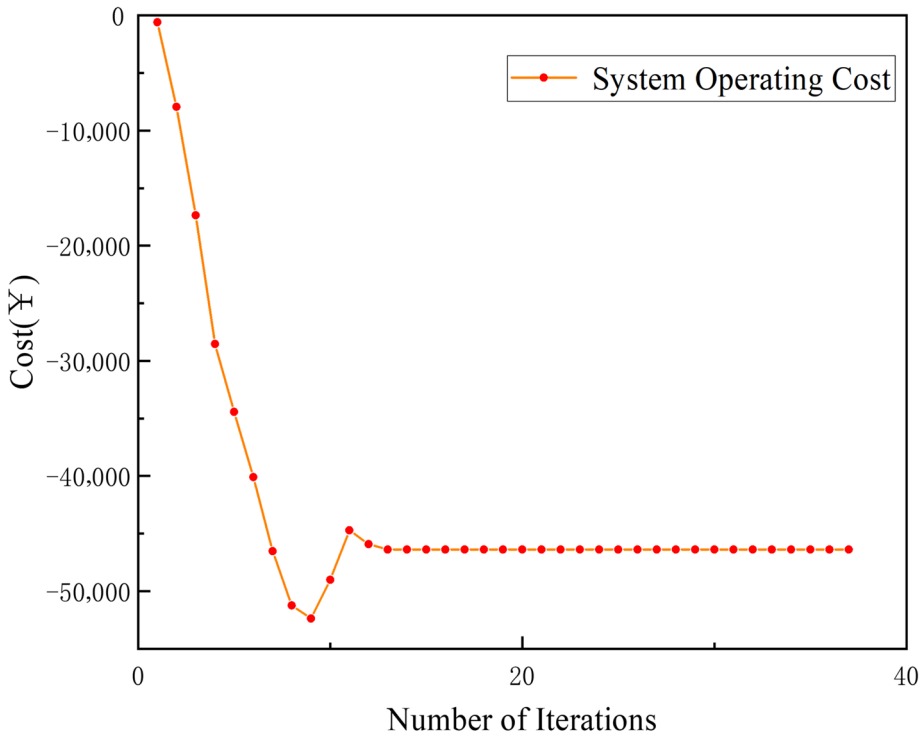

Figure 14. ADMM algorithm iteration results.

The scheduling operation costs and load shedding results for Scenario 1 and Scenario 2 are shown in Table 3. Compared to Scenario 1, Scenario 2, which considers air conditioning load response potential, leads to a reduction in the system operating cost from CNY 50,694.58 to CNY 47,131.64, a 7.6% decrease; and a reduction in load shedding from 1466.35 kWh to 257.31 kWh, a 82% decrease. These results demonstrate that air conditioning loads can significantly reduce the energy burden of the BMG system, while also exhibiting effective peak-shaving and valley-filling characteristics.

Table 3. Scheduling operation cost and load shedding results.

Scenario	System Operating Cost	Load Shedding
Scenario 1	50,694.58	1466.35
Scenario 2	47,131.64	257.31

3.4.2. Analysis of Scheduling Results Under Different Compensation Prices

The total operating cost of the BMG system and the cumulative response power of air conditioning loads under different compensation prices are shown in Figure 15. As the compensation price for air conditioning load scheduling increases, the total operating cost

of the BMG system also increases. Correspondingly, when the compensation price exceeds the peak electricity price of CNY 0.82, the total regulated power of air conditioning loads scheduled by BMO decreases.

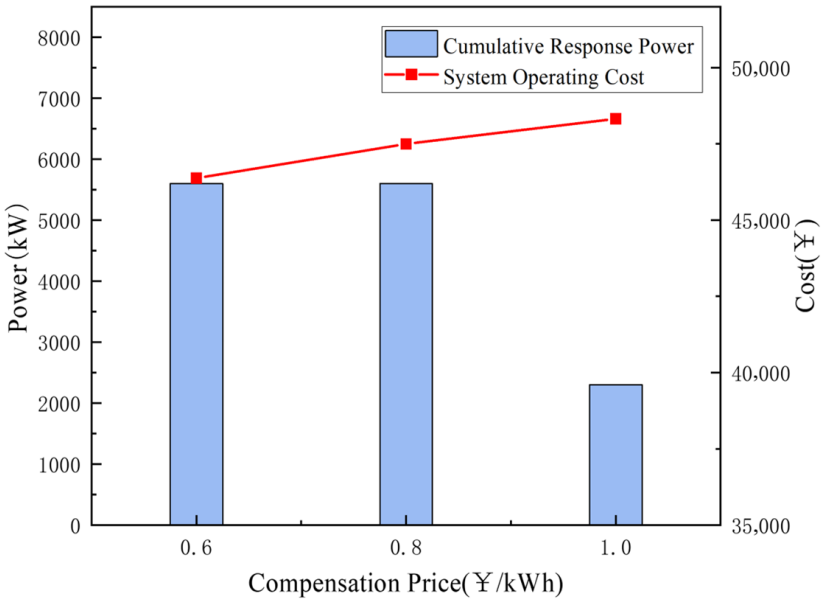

Figure 15. Air conditioning response power and operating cost under different compensation prices.

Figure 16 shows the power reduction in air conditioning loads during different time periods when the compensation price is set to 0.6 and 1. When the compensation price exceeds the peak electricity price of CNY 0.82, the response power of air conditioning loads scheduled by the BMG decreases. Under this condition, air conditioning loads only respond during periods when load losses occur.

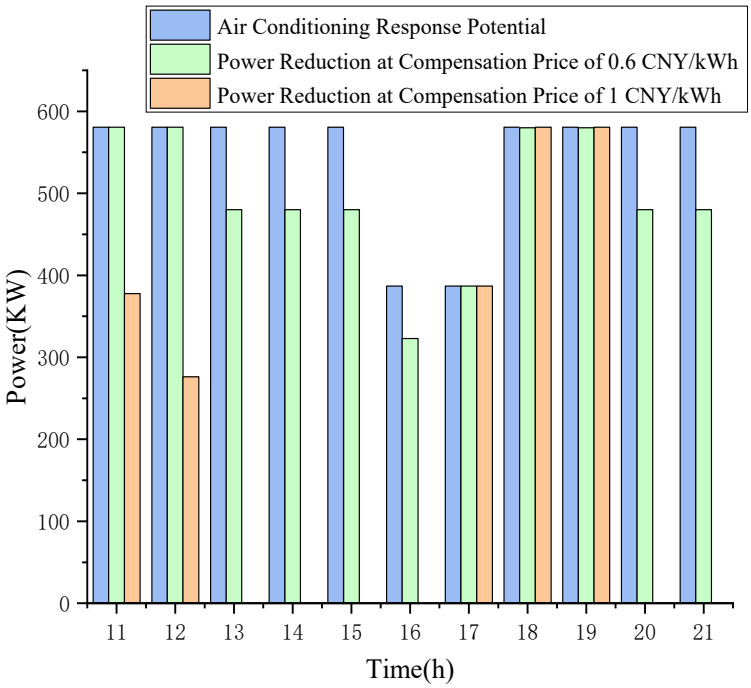

Figure 16. Power reduction at different time periods under various compensation prices.

3.5. Simulation Analysis of the Real-Time Air Conditioning Control Strategy

According to the content in Section 2.5 of this paper, to ensure the effectiveness of regulation, the K-means clustering algorithm is applied using the features P_{int}, $-1/A_4$,

B_1/A_4, and B_2/A_4 to cluster air conditioning loads into different aggregation groups and calculate the capacity of each group. Each group is assigned scheduling tasks proportionally based on its aggregated capacity. The LA performs regulation on each aggregation group according to the allocated scheduling tasks. The clustering results are presented in Table 4.

Table 4. Clustering grouping results.

Group	P_{int}	$-1/A_4$	B_1/A_4	B_2/A_4	Number of Users
1	1.69	2.70	0.84	−41.06	1832
2	1.67	2.69	0.57	−41.21	1656
3	1.71	2.71	1.09	−41.38	1512

This paper analyzes the air conditioning load task of 580.8 kW scheduled for the 13:00–14:00 time slot assigned to Group 1. After capacity allocation, the scheduling task for Group 1 is 212.7 kW. Based on the temperature ranges determined in the response-potential evaluation, the load aggregator (LA) establishes contract groups for Group 1, where the upper and lower temperature bounds of each contract group increase in increments of 0.5 °C. Users select and sign contracts for the appropriate temperature regulation intervals according to their willingness to respond, implying that the initial temperature distribution varies among users within different contract groups. Each contract group is divided into 10 temperature intervals based on the state queue model. The contract parameters and the number of signed users are presented in Table 5.

Table 5. Contract parameters for signed users.

Contract Group	Temperature Interval	Adjustable Capacity	Contracted Users
1	[24.5, 26.5]	713.38	573
2	[25, 27]	660.96	712
3	[25.5, 27.5]	601.70	547

Based on the above-allocated scheduling tasks, the number of loads required to participate in regulation for each contract group can be calculated using Equation (40), from which the parameter τ is derived. The required regulation load quantities for each contract group in the sparse state interval are listed in Table 6.

Table 6. Regulation load demand for sparse modules in each contract group.

Group	Response Quantity	τ	State Group			
			1	2	6	7
1	70	7	7	2	0	0
3	54	6	0	0	1	6

Using the proposed control strategy, regulation is applied to three contract groups. The load transfer quantities in each contract group are calculated based on Equations (42) and (43), and the results are shown in Table 7.

Table 7. Load quantity state transition results.

Group	State Transition Results [Quantity, Time (min)}			
	3-1	3-2	5-6	5-7
1	7, 2.41	2, 1.15	0, 0	0, 0
3	0, 0	0, 0	1, 3.39	6, 1.95

From Table 7, the load transfer results for each contract group are as follows: in Contract Group 1, the load shortages in Temperature Modules 1 and 2 are compensated by transferring seven and two loads, respectively, from Module 3. The corresponding transfer times are 2.41 min and 1.15 min. In Contract Group 3, the load shortages in Temperature Modules 6 and 7 are compensated by transferring one and six loads, respectively, from Module 5. The corresponding transfer times are 3.39 min and 1.95 min.

The proposed control strategy is applied to the contract groups within Group 1, and the control performance is illustrated in Figure 17. The horizontal axis in the figure represents the time of the real-time control process, and the vertical axis represents the power reduction amount after air conditioning load aggregation, which is used to reflect the tracking ability, transient-fluctuation size, and steady-state deviation of different control strategies for scheduling peak-shaving tasks.

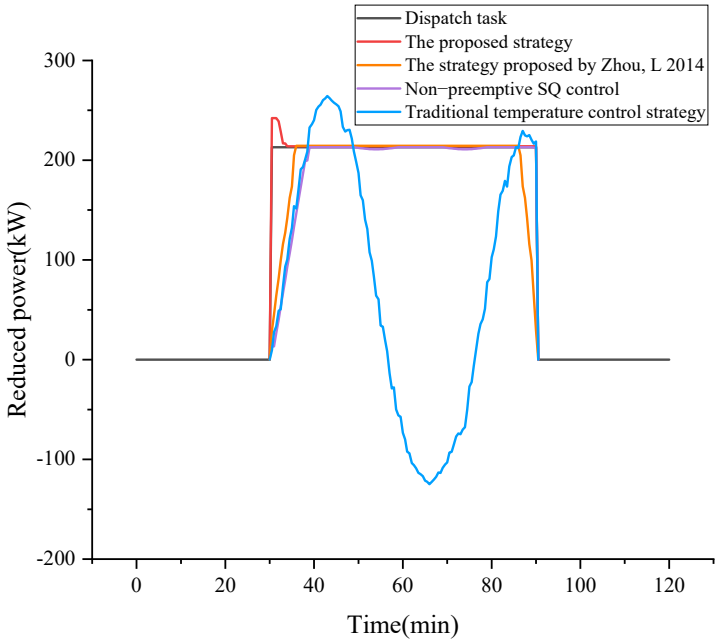

Figure 17. Effectiveness and comparison of control strategies [32].

The proposed control strategy is compared with the traditional temperature control strategy (i.e., reducing the temperature setpoint by 0.5 °C), non-pre-emptive SQ control, and the friendly temperature adjustment strategy based on the state queue model proposed in Ref. [32]. When applying the strategy proposed in this paper, the maximum power fluctuation within the first 3.39 min is 27.04 kW. This is because the objective function is set to minimize the state transition time, allowing a rapid advance transfer from dense to sparse states toward the idealized distribution of the state queue model. As a result, the power reduction increases gradually and becomes stable. In contrast, the traditional temperature control strategy—by directly lowering the setpoint—can reduce the load in the initial stage. However, it disrupts the diversity of the state queue model, causing some states to become vacant or disappear. This leads to power rebound phenomena in air conditioning loads, resulting in significant power fluctuations and subsequent periodic oscillations. The overall response process of non-pre-emptive SQ control is relatively stable and can avoid the obvious rebound caused by traditional temperature control. However, the speed of achieving the target power reduction in the initial stage of scheduling is relatively slow, and there is a certain transient tracking lag. As for the control strategy in Ref. [32], upon receiving the scheduling task, it takes approximately 5 min to reach the target power reduction, during which a certain degree of response deviation occurs. To evaluate the impact of parameter sampling and initial-state uncertainty on the results, we

conducted multiple independent runs under identical settings using different random seeds. The results show that the variations in key metrics are limited, and the relative ranking of different control strategies, as well as the main conclusions, remain consistent. From the above comparison, it can be concluded that the proposed strategy in this paper can rapidly and effectively reduce power fluctuations. It enables a more uniform distribution of load across different temperature states in the state queue during peak-shaving response, thereby effectively mitigating load volatility and minimizing response deviation.

4. Conclusions

This study addresses the issues of dispersion and response fluctuation of air conditioning loads in BMG systems and proposes a day-ahead and real-time coordinated aggregation control strategy for air conditioning loads in BMG. The conclusions drawn from the case study are as follows:

(1) The proposed day-ahead and real-time aggregated control framework for air conditioning loads can effectively exploit the response potential of air conditioning loads. By co-optimizing the scheduling and control layers, it achieves coordinated, flexible, and precise control in tracking the scheduling plan, thereby enhancing system stability and reliability.

(2) In terms of load modeling, an approximated model of air conditioning loads is developed based on a single-zone RC model of buildings, incorporating the thermal transfer characteristics of buildings. The model fully accounts for the influence of external environmental factors on aggregated power and introduces user comfort and willingness indices to further explore the multi-factor aggregation response potential of building air conditioning loads, providing a foundation for day-ahead scheduling.

(3) At the day-ahead scheduling layer, the flexible regulation characteristics of air conditioning load clusters during peak load periods are fully utilized to established a BMO-LA day-ahead distributed-scheduling model. By adopting an ADMM-based distributed strategy, the model effectively reduces system operation costs and load losses without compromising user information privacy.

(4) At the real-time control layer, a pre-emptive air conditioning load control strategy based on the SQ model is proposed. This approach effectively mitigates power fluctuations caused by uneven initial temperature distributions of air conditioners, achieves refined control of air conditioning loads, and further ensures the supply–demand balance of the BMG system.

The proposed control strategy provides a new perspective for flexible load management in integrated BMG systems. Future research can investigate aggregated air conditioning load control under multi-source uncertainties to enable more comprehensive intelligent energy management for BMGs. Meanwhile, a multi-dimensional satisfaction evaluation framework can be introduced by constructing calibratable satisfaction curves for thermal comfort, economic benefits, and privacy preferences, and then achieving trade-offs among these dimensions through multi-objective optimization or risk-constrained decision-making. In addition, for large-scale deployment, it is worth exploring engineering acceleration and communication-overhead reduction strategies such as hierarchical ADMM, and integrating data-driven forecasting models to improve the robustness and generalizability of day-ahead scheduling and real-time control.

Author Contributions: Methodology, J.D., W.D., B.X., D.H., D.Q., H.W. and Z.T.; software, J.D. and W.D.; validation, B.X.; formal analysis, D.H.; investigation, D.Q.; resources, J.D.; data curation, B.X.; writing—original draft preparation, W.D.; writing—review and editing, D.Q.; funding acquisition, D.Q. All authors have read and agreed to the published version of the manuscript.

Funding: This project was supported by the State Grid Anhui Electric Power Co., Ltd.: Science and Technology Project (B3120524003L).

Data Availability Statement: The data presented in this study are available on request from the corresponding author.

Conflicts of Interest: Authors Jinjin Ding, Wangchao Dong, Bin Xu and Dan Hu were employed by the State Grid Anhui Electric Power Research Institute. The remaining authors declare that the research was conducted in the absence of any commercial or financial relationships that could be construed as a potential conflict of interest. State Grid Anhui Electric Power Co., Ltd. had no role in the design of the study; in the collection, analyses, or interpretation of data; in the writing of the manuscript, or in the decision to publish the results.

Abbreviations

C_w	Heat capacity effect caused by wall thickness
C_{in}	Heat capacity effect caused by indoor space
T_{wall}	Wall temperature
T_{in}	Indoor temperature
T_{out}	Outer node temperature
$R_{\text{in}}^{\text{wall}}$	Internal thermal resistance of the wall
$R_{\text{out}}^{\text{wall}}$	External thermal resistance of the wall
γ	Light absorption of building walls
A	Surface area of the building's external wall
Q_{rad}^{wall}	Light intensity corresponding to the wall
ξ_{in}	Window existence coefficient
$R_{w,\text{in}}$	Window thermal resistance
γ^w	Light transmittance of windows
$A^{w,\text{in}}$	Building window area
$Q_{rad}^{w,\text{in}}$	Light intensity corresponding to the windows
m_t	Air conditioning load switch state
β_{sea}	Seasonal coefficient
Q_{int}	Cooling (heating) power of air conditioning equipment
η	Coefficient of Performance (COP)
T_{set}	Air conditioning temperature setpoint
δ	Control dead zone of air conditioning
t_o	Start-up time
t_c	Shutdown time
P_{agg}^t	Aggregated power of the air conditioning load cluster
$p_{\text{on},i}$	Probability of the *i-th* air conditioning load in the cluster being in the on state
T_{com}	Optimal comfortable temperature
$I_{\text{PMV},t}$	PMV value of indoor users at time t
T_{sk}	Average skin temperature when the human body feels comfortable
edu	User education level
I	Household income
A_{age}	Average age of household users
$\Delta T_{i,t}$	Temperature adjustment variation in the *i-th* air conditioning equipment at time t considering user willingness factors
$\Delta P_{\text{ac},t}$	Response potential of the air conditioning cluster
$C_{\text{grid},t}$	Power purchase price from the power grid
$P_{\text{grid},t}$	Power purchase volume from the power grid
C_{ess}	Energy storage equipment charging and discharging cost coefficient
C_{ac}	Compensation price per unit of electricity for air conditioning loads
$P_{\text{ac},t}$	Target power of air conditioning loads
C_{loss}	Load loss penalty price
$P_{\text{loss},t}$	Load loss electricity
$P_{\text{ess},t}^C$	Energy storage charging power
$P_{\text{ess},t}^D$	Energy storage discharging power
$P_{\text{PV},t}$	Photovoltaic predicted output
$P_{l,t}$	Load demand at time t
$\chi_{C,t}$	Energy storage equipment charging state
$\chi_{D,t}$	Energy storage equipment discharging state
η_{ess}^C	Energy storage charging efficiency
η_{ess}^D	Energy storage discharging efficiency
λ_ρ	Lagrange multiplier
ρ_P	Penalty parameter
$\overline{P}_{\text{int},t}$	Average value of coupled variables between the two subproblems
$n_{\text{close},k}$	Number of loads to be controlled in each contract group
$n_{\text{on},m}$	Number of air conditioning loads in the m-th temperature interval
n_{sparse}	Number of sparse intervals
$T_{\text{sparse,up},m}$	Maximum temperature of the queue module in the *m-th* sparse state
$T_{\text{dense,up},m_1}$	Maximum temperature of the queue module in the m_1-*th* dense state

I_{cl}	Clothing thermal resistance	T_{tran,m_1}	Temperature after load transfer in the m_1-*th* state
φ_1	Education level coefficient	T_{later,m_1}	Temperature of the m_1-*module* after transition
φ_2	Household income coefficient	n_d	Number of loads transferred($T_{sparse,\mathrm{up,m}} < T_{\mathrm{dense,up,m_1}}$)
φ_3	Average age coefficient	$\Delta t_{\mathrm{d,m}}$	The load transfer time for each load in $\mathrm{n_d}$
φ	Subjective response coefficient	n_s	Number of loads transferred($T_{sparse,\mathrm{up,m}} > T_{\mathrm{dense,up,m_1}}$)
$\mu_{i,t}$	User willingness impact factor	$\Delta t_{\mathrm{s,m}}$	The load transfer time for each load in $\mathrm{n_s}$
$\omega_1, \omega_2, \omega_3$	User education level increases from high to low	ω_4	Threshold of user willingness given household income
ω_5	average age of the user group		

References

1. Cheng, Z.; Yao, Z. A novel approach to predict buildings load based on deep learning and non-intrusive load monitoring technique, toward smart building. *Energy* **2024**, *312*, 133456. [CrossRef]
2. Karbasforoushha, M.A.; Khajehzadeh, M.; Jearsiripongkul, T.; Keawsawasvong, S.; Eslami, M. A comprehensive review of building energy optimization using metaheuristic algorithms. *J. Build. Eng.* **2024**, *98*, 111377. [CrossRef]
3. Wang, C.; Wang, B.; You, F. Demand response for residential buildings using hierarchical nonlinear model predictive control for plug-and-play. *Appl. Energy* **2024**, *369*, 123581. [CrossRef]
4. Zheng, Z.; Tang, R.; Luo, X.; Li, H.; Wang, S. A Distributed Coordination Strategy for Heterogeneous Building Flexible Thermal Loads in Responding to Smart Grids. *IEEE Trans. Smart Grid* **2024**, *15*, 1620–1633. [CrossRef]
5. Waseem, M.; Lin, Z.; Liu, S.; Zhang, Z.; Aziz, T.; Khan, D. Fuzzy compromised solution-based novel home appliances scheduling and demand response with optimal dispatch of distributed energy resources. *Appl. Energy* **2021**, *290*, 116761. [CrossRef]
6. Du, Y.; Zandi, H.; Kotevska, O.; Kurte, K.; Munk, J.; Amasyali, K.; Mckee, E.; Li, F. Intelligent multi-zone residential HVAC control strategy based on deep reinforcement learning. *Appl. Energy* **2021**, *281*, 116117. [CrossRef]
7. Ostadijafari, M.; Dubey, A.; Yu, N. Linearized Price-Responsive HVAC Controller for Optimal Scheduling of Smart Building Loads. *IEEE Trans. Smart Grid* **2020**, *11*, 3131–3145. [CrossRef]
8. Mahmud, A.; Dhrubo, E.A.; Ahmed, S.S.; Chowdhury, A.H.; Hossain, F.; Rahman, H.; Masood, N.-A. Energy conservation for existing cooling and lighting loads. *Energy* **2022**, *255*, 124588. [CrossRef]
9. Ding, Y.; Zhang, H.; Yang, X.; Tian, Z.; Huang, C. An adaptive switching control model for air conditioning systems based on information completeness. *Appl. Energy* **2024**, *375*, 124004. [CrossRef]
10. Gao, Y.; Li, S.; Fu, X.; Dong, W.; Lu, B.; Li, Z. Energy management and demand response with intelligent learning for multi-thermal-zone buildings. *Energy* **2020**, *210*, 118411. [CrossRef]
11. Fu, Y.; O'Neill, Z.; Wen, J.; Pertzborn, A.; Bushby, S.T. Utilizing commercial heating, ventilating, and air conditioning systems to provide grid services: A review. *Appl. Energy* **2022**, *307*, 118133. [CrossRef]
12. Jiang, L.; Yao, R.; Liu, K.; McCrindle, R. An Epistemic-Deontic-Axiologic (EDA) agent-based energy management system in office buildings. *Appl. Energy* **2017**, *205*, 440–452. [CrossRef]
13. Kim, J.; Yoo, Y.-S.; Yang, H.S.; Choi, H.S. Robust uncertainty-aware control of energy storage systems using biased renewable energy forecast. *Appl. Energy* **2024**, *367*, 123309. [CrossRef]
14. Pinto, G.; Kathirgamanathan, A.; Mangina, E.; Finn, D.P.; Capozzoli, A. Enhancing energy management in grid-interactive buildings: A comparison among cooperative and coordinated architectures. *Appl. Energy* **2022**, *310*, 118497. [CrossRef]
15. Rosales-Asensio, E.; De Simón-Martín, M.; Borge-Diez, D.; Blanes-Peiró, J.J.; Colmenar-Santos, A. Microgrids with energy storage systems as a means to increase power resilience: An application to office buildings. *Energy* **2019**, *172*, 1005–1015. [CrossRef]
16. Rohács, D. Analysis and optimization of potential energy sources for residential building application. *Energy* **2023**, *275*, 127508. [CrossRef]
17. Ding, Y.; Sun, X.; Ruan, J.; Shi, W.; Wu, H.; Xu, Z. Customized decentralized autonomous organization based optimal energy management for smart buildings. *Appl. Energy* **2024**, *376*, 124223. [CrossRef]
18. Luo, J.; Panchabikesan, K.; Lai, K.; Olawumi, T.O.; Mewomo, M.C.; Liu, Z. Game-theoretic optimization strategy for maximizing profits to both end-users and suppliers in building rooftop PV-based microgrids. *Energy* **2024**, *313*, 133715. [CrossRef]
19. Utama, C.; Troitzsch, S.; Thakur, J. Demand-side flexibility and demand-side bidding for flexible loads in air-conditioned buildings. *Appl. Energy* **2021**, *285*, 116418. [CrossRef]
20. Pinzon, J.A.; Vergara, P.P.; Da Silva, L.C.P.; Rider, M.J. Optimal Management of Energy Consumption and Comfort for Smart Buildings Operating in a Microgrid. *IEEE Trans. Smart Grid* **2019**, *10*, 3236–3247. [CrossRef]

21. Rezaei, E.; Dagdougui, H. Optimal Real-Time Energy Management in Apartment Building Integrating Microgrid With Multizone HVAC Control. *IEEE Trans. Ind. Inform.* **2020**, *16*, 6848–6856. [CrossRef]
22. Alzahrani, A.; Sajjad, K.; Hafeez, G.; Murawwat, S.; Khan, S.; Khan, F.A. Real-time energy optimization and scheduling of buildings integrated with renewable microgrid. *Appl. Energy* **2023**, *335*, 120640. [CrossRef]
23. Rigo-Mariani, R.; Ahmed, A. Coordinated management under uncertainty and fair revenue distribution in a multi energy community. *Energy* **2025**, *339*, 138802. [CrossRef]
24. Nematkhah, F.; Bahrami, S.; Aminifar, F.; Catalao, J.P.S. Exploiting the Potentials of HVAC Systems in Transactive Energy Markets. *IEEE Trans. Smart Grid* **2021**, *12*, 4039–4048. [CrossRef]
25. Cui, W.; Ding, Y.; Hui, H.; Lin, Z.; Du, P.; Song, Y.; Shao, C. Evaluation and Sequential Dispatch of Operating Reserve Provided by Air Conditioners Considering Lead–Lag Rebound Effect. *IEEE Trans. Power Syst.* **2018**, *33*, 6935–6950. [CrossRef]
26. Wang, Y.; Tang, Y.; Xu, Y. A Distributed Control Scheme of Thermostatically Controlled Loads for the Building-Microgrid Community. *IEEE Trans. Sustain. Energy* **2020**, *11*, 350–360. [CrossRef]
27. Rama Curiel, J.A.; Thakur, J. A novel approach for Direct Load Control of residential air conditioners for Demand Side Management in developing regions. *Energy* **2022**, *258*, 124763. [CrossRef]
28. Lu, N.; Zhang, Y. Design Considerations of a Centralized Load Controller Using Thermostatically Controlled Appliances for Continuous Regulation Reserves. *IEEE Trans. Smart Grid* **2013**, *4*, 914–921. [CrossRef]
29. Zhou, T.; Chen, H.; Zhang, N.; Han, Y.; Zhou, S.; Li, Z.; Zhou, M. An analogue on/off state-switching control method suitable for inverter-based air conditioner load cluster participating in demand response. *Appl. Energy* **2024**, *363*, 123096. [CrossRef]
30. *ISO 7730:2025*; Ergonomics of the Thermal Environment—Analytical Determination and Interpretation of Thermal Comfort Using Calculation of the PMV and PPD Indices and Local Thermal Comfort Criteria. International Organization for Standardization (ISO): Geneva, Switzerland, 2025.
31. Wang, B.; Cai, Q.; Sun, Z. Determinants of willingness to participate in urban incentive-based energy demand-side response: An empirical micro-data analysis. *Sustainability* **2020**, *12*, 8052. [CrossRef]
32. Zhou, L.; Li, Y.; Gao, C.W. Improvement of temperature adjusting method for aggregated air-conditioning loads and its control strategy. *Proc. CSEE* **2014**, *34*, 5579–5589. [CrossRef]

Disclaimer/Publisher's Note: The statements, opinions and data contained in all publications are solely those of the individual author(s) and contributor(s) and not of MDPI and/or the editor(s). MDPI and/or the editor(s) disclaim responsibility for any injury to people or property resulting from any ideas, methods, instructions or products referred to in the content.